Ferroptosis is controlled by the coordinated transcriptional regulation of glutathione and labile iron metabolism by the transcription factor BACH1

Received for publication, May 28, 2019, and in revised form, November 12, 2019 Published, Papers in Press, November 18, 2019, DOI 10.1074/jbc.RA119.009548

Hironari Nishizawa[‡], Mitsuyo Matsumoto[‡§], Tomohiko Shindo[¶], Daisuke Saigusa[‖], Hiroki Kato[‡], Katsushi Suzuki[‡], Masaki Sato[‡], Yusho Ishii[‡], Hiroaki Shimokawa[¶], and Kazuhiko Igarashi[‡§1]

From the [‡]Department of Biochemistry, [§]Center for Regulatory Epigenome and Diseases, and [¶]Department of Cardiovascular Medicine, Tohoku University Graduate School of Medicine, Seiryo-machi 2-1, Sendai 980-8575, Japan and the [‖]Department of Integrative Genomics, Tohoku University Tohoku Medical Megabank Organization, Seiryo-machi 2-1, Sendai 980-8573, Japan

Edited by Joel M. Gottesfeld

Ferroptosis is an iron-dependent programmed cell death event, whose regulation and physiological significance remain to be elucidated. Analyzing transcriptional responses of mouse embryonic fibroblasts exposed to the ferroptosis inducer erastin, here we found that a set of genes related to oxidative stress protection is induced upon ferroptosis. We considered that up-regulation of these genes attenuates ferroptosis induction and found that the transcription factor BTB domain and CNC homolog 1 (BACH1), a regulator in heme and iron metabolism, promotes ferroptosis by repressing the transcription of a subset of the erastin-induced protective genes. We noted that these genes are involved in the synthesis of GSH or metabolism of intracellular labile iron and include *glutamate-cysteine ligase modifier subunit* (*Gclm*), *solute carrier family 7 member 11* (*Slc7a11*), *ferritin heavy chain 1* (*Fth1*), *ferritin light chain 1* (*Ftl1*), and *solute carrier family 40 member 1* (*Slc40a1*). Ferroptosis has also been previously shown to induce cardiomyopathy, and here we observed that *Bach1*$^{-/-}$ mice are more resistant to myocardial infarction than WT mice and that the severity of ischemic injury is decreased by the iron-chelator deferasirox, which suppressed ferroptosis. Our findings suggest that BACH1 represses genes that combat labile iron-induced oxidative stress, and ferroptosis is stimulated at the transcriptional level by BACH1 upon disruption of the balance between the transcriptional induction of protective genes and accumulation of iron-mediated damage. We propose that BACH1 controls the threshold of ferroptosis induction and may represent a therapeutic target for alleviating ferroptosis-related diseases, including myocardial infarction.

Ferroptosis is a new form of programmed cell death caused by the iron-dependent accumulation of lipid hydroperoxide (1, 2). As a pathological cell death, ferroptosis causes various oxidative stress-related diseases, including ischemia-reperfusion injury (3–7) and neurodegenerative diseases (8, 9). Ferroptosis also contributes to tumor suppression as a response induced by p53 and is important for organisms in preventing cancer (2, 10–13). Considering the involvement of lipid hydroperoxide, ferroptosis may be executed at the edge of the oxidative stress response. Therefore, ferroptosis may be a regulated process involving the oxidative stress response. However, the regulatory mechanism underlying ferroptosis has yet to be elucidated in full. In particular, it is not known at all how the regulatory genes of ferroptosis are transcriptionally controlled in induction of ferroptosis.

BTB and CNC homology 1 (BACH1)[2] is a heme-binding transcription factor required for the proper regulation of the oxidative stress response and metabolic pathways related to heme and iron (14). BACH1 represses *Hmox1* encoding heme oxygenase-1 (HO-1), *Fth1* and *Ftl1* encoding ferritin proteins, *Gclm* and *Gclc* encoding glutamate-cysteine ligase modifier and catalytic subunits, and other genes involved in the oxidative stress response (15–17). We hypothesized that BACH1 might regulate ferroptosis by inhibiting the expression of these genes. In addition, although BACH1 is involved in the exacerbation of various diseases involving oxidative stress, such as ischemic heart disease (18), hyperoxic lung injury (19), trinitrobenzene sulfonic acid-induced colitis (20), nonalcoholic steatohepatitis (21), and spinal cord injury (22), it is unknown whether or not they are attributable to ferroptosis. We considered that BACH1 may exacerbate the severity of these diseases through ferroptosis.

To understand the regulatory mechanism underlying ferroptosis, we analyzed the transcriptome response in ferroptotic cells with RNA-Sequence (RNA-Seq). We also examined

This work was supported in part by Grants-in-Aid from the Japan Society for the Promotion of Science 19K07680 and 16K07108 (to M. M.) and 15H02506, 24390066, 21249014, and 18H04021 (to K. I.) and Agency for Medical Research and Development Grant JP16gm050001 (to K. I.). H. Nishizawa received DFX as raw material from Novartis Pharma for this study. The authors declare that they have no conflicts of interest with the contents of this article.

This article contains Figs. S1–S10, Tables S1–S3, and Movie S1

The RNA-seq data has been deposited at the GEO database under accession code GSE131444.

[1] To whom correspondence should be addressed: Dept. of Biochemistry, Tohoku University Graduate School of Medicine, Seiryo-machi 2-1, Sendai 980-8575, Japan. Tel.: 81-22-717-7596; Fax: 81-22-717-7598; E-mail: igarashi@med.tohoku.ac.jp.

[2] The abbreviations used are: BACH1, BTB and CNC homology 1; HO-1, heme oxygenase-1; MEF, mouse embryonic fibroblast; AMI, acute myocardial infarction; DFX, deferasirox; PI, propidium iodide; DFO, deferoxamine; qPCR, quantitative PCR; LAD, left anterior descending coronary artery; UHPLC, ultra HPLC; P7, passage 7; HBSS, Hank's balanced salt solution; GAPDH, glyceraldehyde-3-phosphate dehydrogenase; ANOVA, analysis of variance; RNA-Seq, RNA-sequence.

whether or not BACH1 was involved in the regulation of ferroptosis by comparing ferroptosis and the expression of ferroptosis-induced genes between wildtype (WT) and *Bach1*$^{-/-}$ mouse embryonic fibroblasts (MEFs). Furthermore, we assessed the influence of BACH1 and ferroptosis on the severity of acute myocardial infarction (AMI) in model mice. We found that BACH1 promoted ferroptosis by directly repressing genes involved in the synthesis of glutathione (GSH) and sequestration of free labile iron. BACH1 also increased the severity of AMI, which was mitigated by the iron chelator deferasirox (DFX). Our findings highlight the coordinated transcriptional response and its regulation by BACH1 upon ferroptosis.

Results

Regulatory genes of ferroptosis show compensatory up-regulation in ferroptotic cells

Changes in metabolic and biological processes occur in ferroptotic cells (23, 24). To determine the changes in transcriptome upon ferroptosis, we treated MEFs with erastin, a class I ferroptosis inducer (1, 2), and carried out RNA-seq analyses. Genes related to oxidative stress and iron metabolism showed significant induction in their expression (Fig. 1*A*). Many of these genes, for example, *Slc7a11, Gclm, Gclc*, are considered to possess inhibitory effects on ferroptosis (25). Therefore, ferroptosis accompanies the induction of genes that can restrict the execution of ferroptosis.

Among the induced genes, *Hmox1* encoding HO-1 is reported to be associated with ferroptosis (26, 27) and is a negatively regulated target of BACH1 (15). *Slc7a11* encodes a component of system x_c^- (cystine/glutamine transporter) (28, 29) and a well-known regulator of ferroptosis (10). *Gclm* and *Gclc* encode glutamate-cysteine ligase modifier and catalytic subunits (30, 31), both considered to suppress ferroptosis by GSH synthesis (25, 32). These genes for the pathway of GSH synthesis are also considered to be targets of BACH1 (17). Indeed, the amount of BACH1 protein was decreased in MEFs exposed to erastin, which was accompanied by the induction of *Hmox1* (Fig. 1, *B* and *C*, and Fig. S1). Although BACH1 protein accumulated after proteasome inhibition by MG132, the degradation of BACH1 in response to erastin was not completely blocked (Fig. 1*D* and *E*). These observations suggest that BACH1 protein is degraded by proteasome-dependent and -independent mechanisms during ferroptosis. With the reduction in BACH1 protein, the production of its mRNA was induced (Fig. S1), suggesting the presence of feedback regulation of BACH1.

These observations suggest that, when cells are exposed to erastin, the expression of genes that counteract ferroptosis is induced in part by a reduction in BACH1 protein and that the amount or activity of BACH1 and the kinetics of its feedback regulation may influence ferroptosis by suppressing this counteracting subprogram of ferroptosis.

BACH1 promotes ferroptosis

To clarify whether or not BACH1 regulates ferroptosis, we treated WT and *Bach1*$^{-/-}$ MEFs with erastin, stained them with propidium iodide (PI) and annexin V, and compared the cell death by a flow cytometry analysis (Fig. S2). *Bach1*$^{-/-}$ MEFs showed less cell death in response to erastin than WT cells (Fig. 2, *A* and *B*). When the erastin-treated MEFs were observed with a transmission electron microscope, mitochondrial spheroids, which reflect oxidative stress (33), were frequently observed in WT MEFs (Fig. 2*C*). Although mitochondrial spheroids were not clear in *Bach1*$^{-/-}$ MEFs exposed to erastin, condensed matrix structures, which are also observed as parts of mitochondrial spheroids (33), were observed (Fig. 2*C*). These results may reflect lower oxidative stress and higher resistance to erastin of *Bach1*$^{-/-}$ MEFs than WT MEFs. The cell death in our experiments was inhibited by the iron chelator deferoxamine (DFO) (Fig. 2, *D* and *E*), confirming that this death was ferroptosis. These results showed that BACH1 promoted ferroptosis in MEFs.

It should be noted that *Bach1*$^{-/-}$ MEFs lost their resistance to ferroptosis under high doses of erastin (Fig. 2, *A* and *B*). Although decreased BACH1 by erastin is considered as a protective response to ferroptosis (Fig. 1, *A*–*C*), there is also its limitation to the inhibition of cell death. However, at least at the early stage, the reduction in BACH1 protein may be a part of the ferroptosis program, and BACH1 may set the threshold for ferroptosis. Execution of ferroptosis may be determined by the basal amount of BACH1 and how rapidly it is degraded in response to ferroptosis inducers.

BACH1 represses the expression of genes involved in the GSH synthesis pathway

GSH is the key regulator of ferroptosis (1, 2) and the genes involved in the pathway of GSH synthesis were up-regulated as BACH1 protein decreases (Fig. 1, *A*–*C*). Therefore, BACH1 may decrease GSH by repressing the expression of these genes. To investigate this possibility, we measured the intracellular GSH concentrations in WT and *Bach1*$^{-/-}$ MEFs. Because the sensitivity to ferroptosis decreased as we passaged MEFs (Fig. S3, *A* and *B*), we performed the measurement of GSH and the subsequent analysis of gene expression at three different stages of primary culture (7th, 9th, and 11th passage; P7, P9, and P11). The amounts of GSH at P7 and P9 were significantly higher in *Bach1*$^{-/-}$ MEFs than in WT cells and a similar trend was observed at P11 (Fig. 3*A*), suggesting that BACH1 promoted ferroptosis by reducing GSH within cells.

By revisiting our previous data of ChIP with sequencing (ChIP-Seq) of BACH1 in mouse myeloblast M1 cells (34, 35), we found peaks of BACH1 and its partner MAFK in the regulatory regions of genes encoding molecules for GSH synthesis, including *Gclm*, *Gclc*, and *Slc7a11* (Fig. 3*B*). Furthermore, by comparing the expression of these genes in WT and *Bach1*$^{-/-}$ MEFs by quantitative PCR (qPCR), the expression of all of these genes was confirmed to be higher in *Bach1*$^{-/-}$ MEFs than in WT cells (Fig. 3*C*). These results suggested that BACH1 bound to the regulatory regions of these genes to repress their expression.

A comparison of the protein amounts of SLC7A11, GCLM, and GCLC in MEFs by Western blotting revealed that more GCLM protein was present in *Bach1*$^{-/-}$ MEFs than in WT cells (Fig. 3, *D* and *E*, and Fig. S4, *A* and *B*). Although the amounts of SLC7A11 protein were similar in WT and *Bach1*$^{-/-}$ MEFs (Fig. 3, *D* and *E*, and Fig. S4, *A* and *B*), more SLC7A11 protein was present in *Bach1*$^{-/-}$ MEFs than in WT cells when they were treated with proteasome inhibitor MG132 (Fig. 3, *D* and *E*).

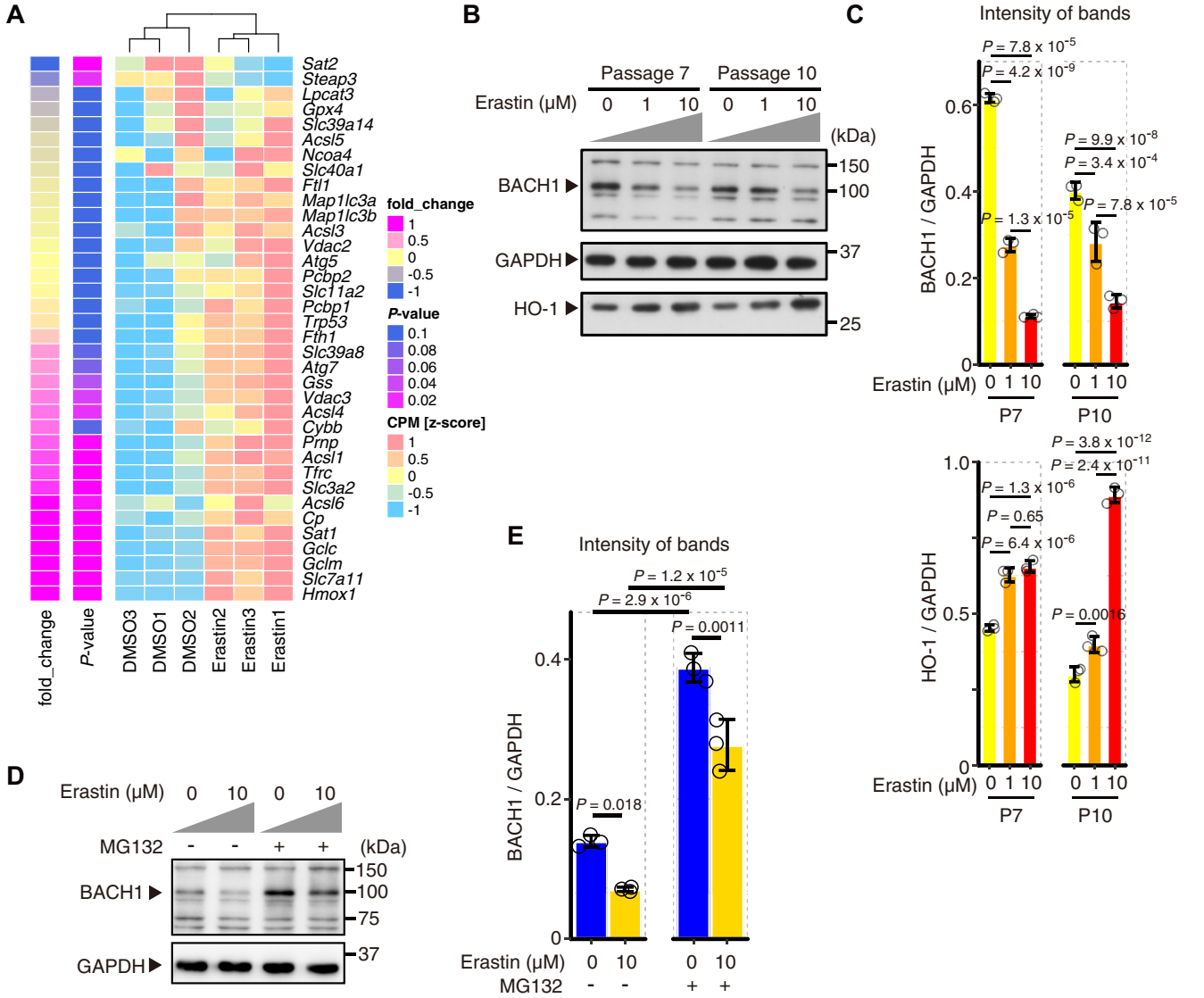

Figure 1. Regulatory genes of ferroptosis are up-regulated with decreased BACH1 protein in the induction of ferroptosis. *A,* RNA-seq was performed in WT MEFs (9th passage: *P9*) with only DMSO (DMSO group) or DMSO + 3 μM erastin (Erastin group) for 24 h. A heat map of gene expression profiles shows the genes registered to map04216 (Ferroptosis pathway) of Kyoto Encyclopedia of Genes and Genomes (KEGG) pathway map. The genes were arranged from the bottom in the order of fold-change of erastin group to DMSO group. $n = 3$ per group. *B* and *C*, Western blotting for BACH1, HO-1, and GAPDH of WT MEFs (7th passage: *P7*, 11th passage: *P11*) exposed to erastin for 12 h. Representative image (*B*) and the intensity of bands (*C*). *D* and *E,* Western blotting for BACH1 and GAPDH in WT MEFs (8th passage) exposed to erastin and 25 μM MG132 for 6 h. Representative image (*D*) and the intensity of bands (*E*). In *A*, *p* value by the differential expression analysis performed on edge R. In *C and E*, *error bars* represent S.D. *p* value by Tukey's test after two-way ANOVA.

These observations suggest that the amount of SLC7A11 protein is further tuned by proteasomal-mediated degradation. There were no marked differences in the amount of GCLC protein with or without MG132 (Fig. 3, *D* and *E,* and Fig. S4, *A* and *B*). BACH1 may affect the expression of GCLC protein under certain circumstances. Given these results, we surmised that BACH1 decreased the amount of GSH by repressing the expression of *Gclm* and in part *Slc7a11*.

Knockdown of the genes in GSH synthesis pathway and Hmox1 increases the sensitivity of ferroptosis

We next examined whether or not the resistance of *Bach1*$^{-/-}$ MEFs against ferroptosis was actually dependent on the increased expression of the genes involved in the GSH synthesis pathway. Although it is not always statistically significant, knockdown of any of *Slc7a11, Gclm,* and *Gclc* resulted in slight but reproducible increases in ferroptosis in both WT and *Bach1*$^{-/-}$ MEFs (Figs. S5, *A–C;* S6, *A–C;* and S7, *A–C*). These results show that the genes involved in the GSH synthesis pathway have inhibitory effects against ferroptosis and suggest that BACH1 promotes ferroptosis by repressing their expression. We next examined the effect of knockdown of *Hmox1*. WT MEFs became more sensitive to ferroptosis by knockdown of *Hmox1* than cells with control knockdown (Figs. S5*D*, S6*D*, and S7*D*). We thus concluded that HO-1 works as an inhibitor of ferroptosis under our experimental conditions. However, the effect of HO-1 to accelerate ferroptosis has also been reported (7, 26). The function of HO-1 in ferroptosis might differ

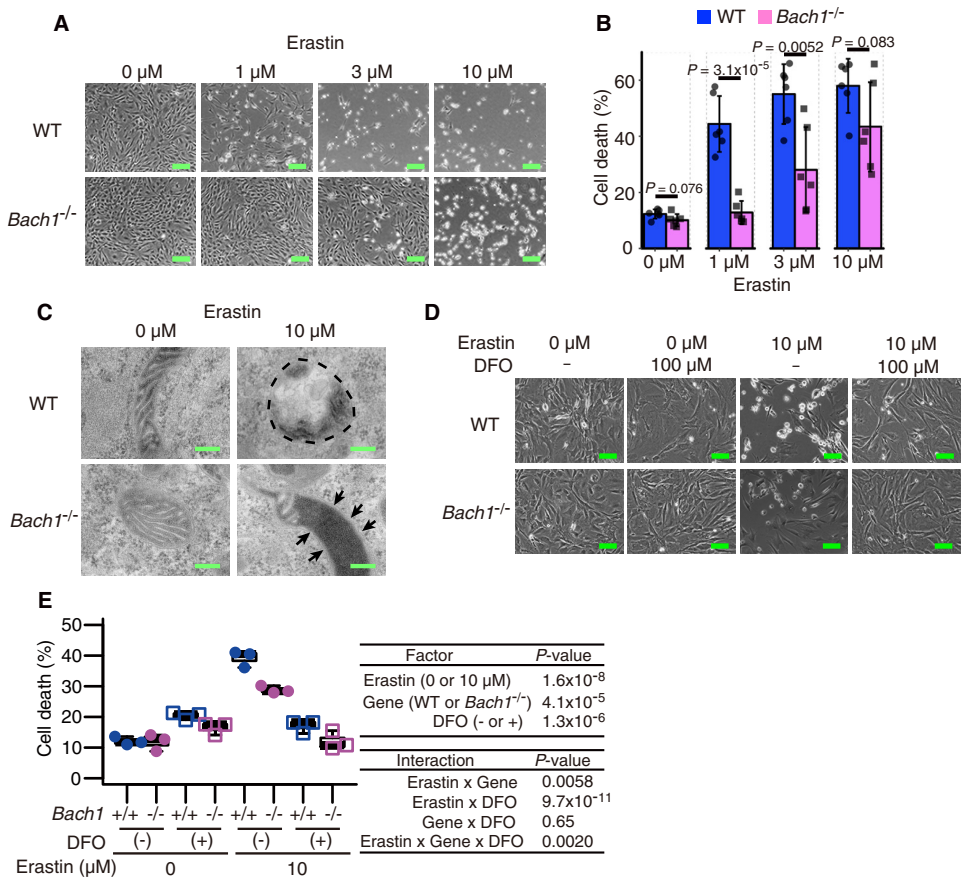

Figure 2. BACH1 promotes ferroptosis. *A* and *B*, optical microscope image (*A*) and quantification of cell death by flow cytometer (*B*) of WT and *Bach1*$^{-/-}$ MEFs (11th passage: *P11*) exposed to erastin for 24 h. *Scale bars* in *A* represent 100 μm. *C*, transmission electron microscope image of WT and *Bach1*$^{-/-}$ MEFs (P9) exposed to erastin for 10 h. The portion surrounded by *dashed line*: a mitochondrial spheroid. *Arrow*: mitochondrial inner membrane-matrix condensation. *Scale bars* represent 200 nm. *D* and *E*, optical microscope image (*D*) and quantification of cell death by flow cytometer (*E*) of WT and *Bach1*$^{-/-}$ MEFs (P12) exposed to erastin and DFO for 24 h. *Scale bars* in *D* represents 200 μm. *A*, *B*, *D*, and *E*, representative of three independent experiments. *Error bars* of *B* represent S.D. The *box and whisker plots* of *E* show the 25th and 75th percentile quartiles and median values (*center black line*) and maximum and minimum values of the data. *p* value of *B* by *t* test. *p* value of *E* by three-way ANOVA.

depending on the situations of cells. Importantly, knockdown of *Slc7a11*, *Gclm*, *Gclc*, or *Hmox1* did not decrease the observed differences in ferroptosis between WT and *Bach1*$^{-/-}$ MEFs (Fig. S7). These results suggest that the role of BACH1 in promoting ferroptosis depends on the repression of multiple genes involved in ferroptosis.

BACH1 accelerates ferroptosis by suppressing labile iron metabolism

To explore other target genes of BACH1 in the regulation of ferroptosis, we examined genes involved in the regulation of iron metabolism (*Fth1*, *Ftl1*, *Slc40a1*, *Tfrc*, *Mfn2*, and *Fxn*), heavy metal stress (*Mt1*), and lipoperoxidation (*Gpx4*). Some of these genes were up-regulated in response to erastin (see Fig. 1*A*). Among these genes, ferritin genes (*Fth1* and *Ftl1*) and the ferroportin gene (*Slc40a1*) were dramatically up-regulated in *Bach1*$^{-/-}$ MEFs (Fig. 4*A*), and binding peaks of BACH1 and MAFK were observed near their regulatory regions (Fig. 4*B*). In contrast, the expression of *Tfrc*, *Mfn2*, *Fxn*, *Mt1*, and *Gpx4* was only mildly increased in *Bach1*$^{-/-}$ MEFs (Fig. S8*A*). There were no strong binding peaks of BACH1 or MAFK in the regulatory regions of these genes (Fig. S8*B*). Considering that both ferritin and ferroportin reduce the availability of free labile iron and are known to inhibit ferroptosis (36–38), these results suggest that BACH1 promotes ferroptosis by repressing the transcription of ferritin and ferroportin genes.

To examine this hypothesis, we measured mitochondrial labile iron in WT and *Bach1*$^{-/-}$ MEFs with a fluorophore Mito-FerroGreen (39). *Bach1*$^{-/-}$ MEFs contained more mitochondrial labile iron than WT without erastin (Fig. 4, *C* and *D*). It is probably due to the effects of HO-1 overexpression. Although prominent increases in labile iron and cell death were observed in WT MEFs in response to erastin, these alterations were much less in *Bach1*$^{-/-}$ MEFs (Fig. 4, *C* and *D*, and Fig. S9, *A* and *B*). These results suggest BACH1 increases mitochondrial labile iron by repressing the transcription of ferritin and ferroportin during ferroptosis. These findings, along with the regulation of GSH synthesis pathway by BACH1, suggest that BACH1 accelerates ferroptosis by decreasing the intracellular activity of GSH and increasing the oxidative activity of labile iron (Fig. 4*E*).

BACH1 aggravates acute myocardial infarction by promoting ferroptosis

Finally, we tried to examine whether or not the promotion of ferroptosis by BACH1 is involved in pathological changes *in*

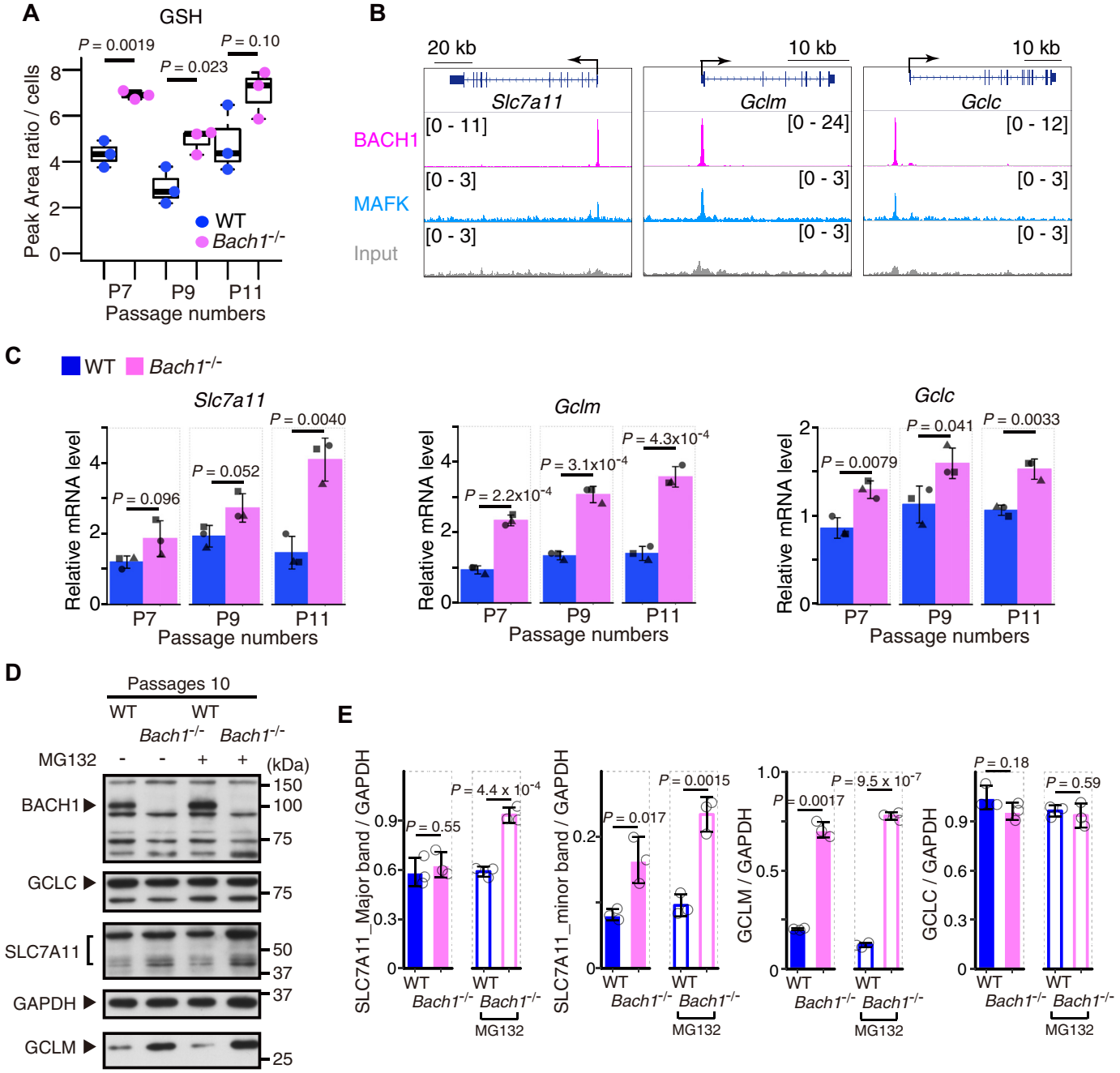

Figure 3. BACH1 decreases GSH by repressing the transcription of *Slc7a11*, *Gclm*, and *Gclc*. *A*, intracellular concentration of GSH in WT and *Bach1*$^{-/-}$ MEFs (7th, 9th, and 11th passage: P7, P9, and P11) by UHPLC/MS/MS. *B*, ChIP-seq analysis of the binding of BACH1, MAFK for gene regions of *Slc7a11*, *Gclm*, and *Gclc* in M1 cells. *C*, qPCR analysis for *Slc7a11*, *Gclm*, and *Gclc* mRNA relative to *Actb* mRNA in WT and *Bach1*$^{-/-}$ MEFs (P7, P9, P11). $n = 3$ of independent lots of MEFs per genotype. *D* and *E*, Western blotting for BACH1, SLC7A11, GCLM, GCLC, and GAPDH in WT and *Bach1*$^{-/-}$ MEFs (P10) exposed to 25 μM MG132. Representative image (*D*) and the intensity of bands (*E*). The *box and whisker plots* of *A* show the 25th and 75th percentile quartiles and median values (*center black line*) and maximum and minimum values of the data. *Error bars* of *C* and *E* represent S.D. *p* value of *A*, *C*, and *E* by *t* test.

vivo. It has long been known that iron and lipid peroxidation are involved in oxidative stress-related cell death, including ischemia-reperfusion injury (40–42). Furthermore, there are several reports showing that ferroptosis is involved in ischemia-reperfusion injury in the heart (3, 4, 7). Therefore, we used an AMI model based on left anterior descending coronary artery (LAD) ligation (43, 44) (Fig. 5*A*). In this model, *Bach1*$^{-/-}$ mice showed less severe injuries than WT mice as judged by the post-operative survival rate and an evaluation of the cardiac function with echocardiography (Fig. 5, *B* and *C*, Fig. S10, *A–C*, and Movie S1, *A–D*). The infarct area on pathological specimens was also smaller in *Bach1*$^{-/-}$ mice than in WT mice (Fig. 5, *D* and *E*). These results suggest that BACH1 exacerbates the pathology of AMI.

To investigate whether or not ferroptosis is involved in the pathology, we observed the myocardial infarct regions using a transmission electron microscope. Mitochondrial spheroid-like abnormality was observed in both WT and *Bach1*$^{-/-}$ mice (Fig. 5*F*). This alteration was consistent with the findings of MEFs exposed to erastin (Fig. 2*C*). We then

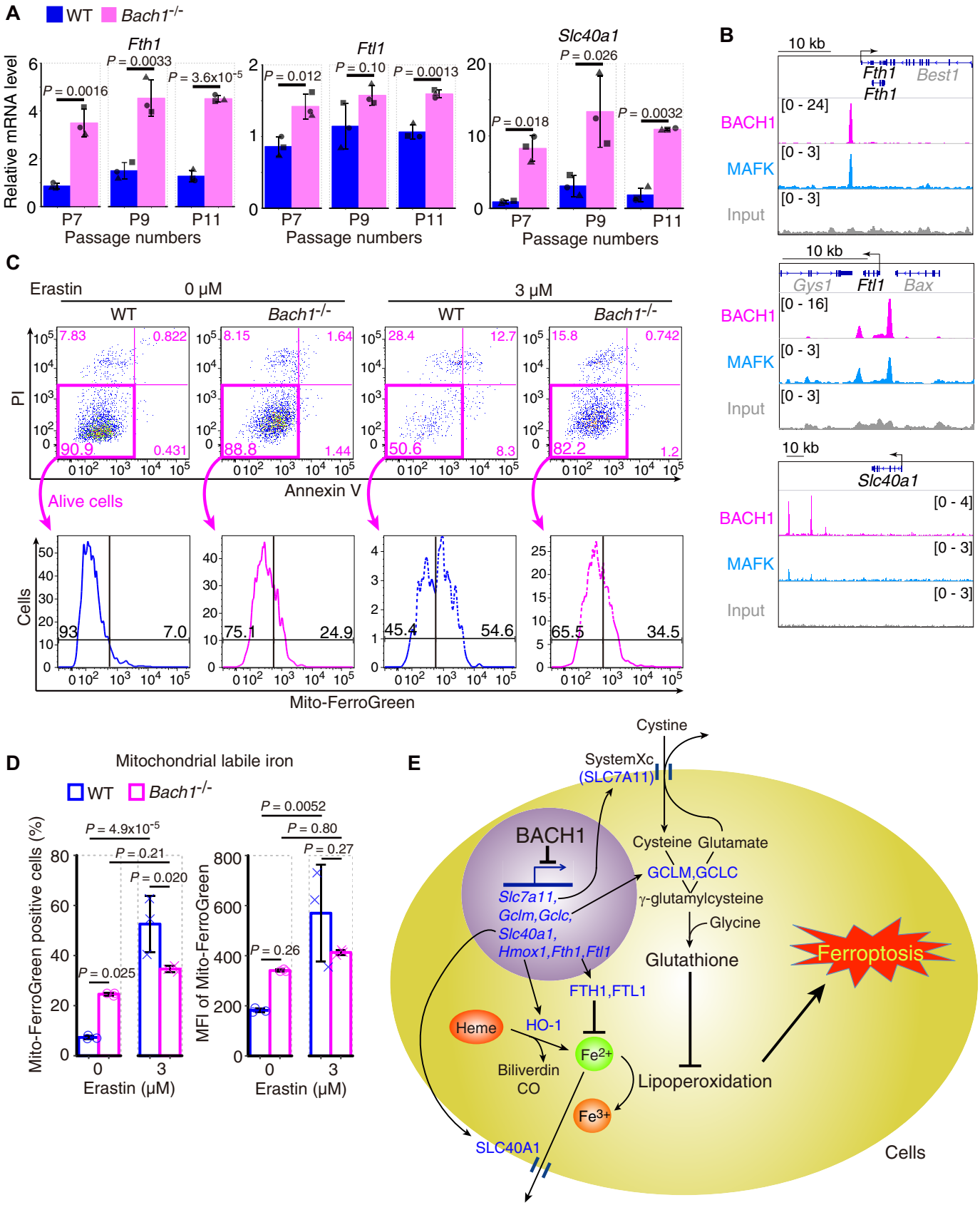
A
WT
Bach1-/-
Fth1
Ftl1
Slc40a1
Relative mRNA level
P = 0.0016
P = 0.0033
P = 3.6x10-5
P = 0.012
P = 0.10
P = 0.0013
P = 0.018
P = 0.026
P = 0.0032
P7
P9
P11
Passage numbers
B
10 kb
Fth1
Best1
[0 - 24]
BACH1
[0 - 3]
MAFK
[0 - 3]
Input
Gys1
Ftl1
Bax
[0 - 16]
Slc40a1
[0 - 4]
C
Erastin
0 μM
3 μM
WT
Bach1-/-
PI
Annexin V
7.83
0.822
90.9
0.431
8.15
1.64
88.8
1.44
28.4
12.7
50.6
8.3
15.8
0.742
82.2
1.2
Alive cells
Cells
93
7.0
75.1
24.9
45.4
54.6
65.5
34.5
Mito-FerroGreen
D
Mitochondrial labile iron
Mito-FerroGreen positive cells (%)
MFI of Mito-FerroGreen
P = 4.9x10-5
P = 0.21
P = 0.020
P = 0.025
P = 0.0052
P = 0.80
P = 0.27
P = 0.26
Erastin (μM)
E
Cystine
SystemXc
(SLC7A11)
BACH1
Slc7a11,
Gclm,Gclc,
Slc40a1,
Hmox1,Fth1,Ftl1
Cysteine
Glutamate
GCLM,GCLC
γ-glutamylcysteine
Glycine
Glutathione
Ferroptosis
FTH1,FTL1
Heme
HO-1
Biliverdin
CO
Fe2+
Fe3+
Lipoperoxidation
SLC40A1
Cells

investigated whether or not the pathological changes could be improved by administering DFX (Fig. 6*A*), which is a clinically used iron chelator. First, we confirmed that it inhibited ferroptosis in MEFs (Fig. S10, *D* and *E*). Although there was no improvement in the survival rates in WT or *Bach1*$^{-/-}$ mice (Fig. 6*B*), an improvement in the cardiac function on echocardiography was observed in the DFX group, which was more prominent in the WT mice than *Bach1*$^{-/-}$ mice (Fig. 6, *C* and *D*, and Fig. S10, *F*–*K*). The DFX group of WT mice showed a reduction in the infarct area; however, no such effect was noted in *Bach1*$^{-/-}$ mice (Fig. 6, *E* and *F*). These results suggest that BACH1 exacerbates the pathology of AMI by promoting ferroptosis.

Discussion

Although genes involved in ferroptosis are being discovered (25), how their expression is regulated during ferroptosis remains unclear. In this study, we found that many of the inhibitory genes of ferroptosis were coordinately up-regulated upon induction of ferroptosis with erastin (Fig. 1*A*). Such a coordinated response may be a mechanism for restricting ferroptosis. We further showed that BACH1 directly counteracted this coordinated response of genes, including *Hmox1*, *Slc7a11*, *Gclm*, *Gclc*, *Fth1*, *Ftl1*, and *Slc40a1* (Figs. 3, *B* and *C*, and 4, *A* and *B*), which are involved in the metabolism of GSH or labile iron. The protein amount of BACH1 was reduced upon the induction of ferroptosis (Fig. 1*B*). Our results suggest that BACH1 is degraded in part by proteasome during ferroptosis (Fig. 1, *D* and *E*). BACH1 is known to be degraded by proteasome under oxidative stress including heme (45–49), therefore the similar mechanism may work in ferroptosis. BACH1 is known to repress the expression of *Slc40a1* in macrophages (50). Therefore, reduction of the BACH1 protein level may trigger the coordinated induction of these genes as a subprogram of the initial phase of ferroptosis program. Cells can then integrate distinct signals leading to BACH1 degradation, and thus judge whether or not they should undergo ferroptosis. Thus, BACH1 sets the threshold for whether or not ferroptosis occurs in response to lipid peroxide synthesized.

NRF2 is known to activate some of the genes that are repressed by BACH1, including *Hmox1, Slc7a11*, *Gclm*, and *Gclc* (51–56). Even though NRF2 increases the intracellular GSH amount, it only weakly protects cells from ferroptosis (57). Other reports have shown that NRF2 can inhibit ferroptosis (27, 58, 59). It is known *Hmox1* is induced by hypoxia inducible factor-1α (Hif-1α) (60, 61) and some reports suggest the possibility that Hif-1α also inhibits ferroptosis (32, 62). Therefore, ferroptosis execution may depend on the initial amounts and kinetics of the induction or reduction of these transcription factors. This mechanism may extend our understanding of the regulation of ferroptosis, wherein ferroptosis is a cell death programmed at the level of the gene regulatory network.

We showed that GSH was higher in *Bach1*$^{-/-}$ MEFs than WT cells (Fig. 3*A*). Our results strongly suggest that BACH1 decreases intracellular GSH by repressing the expression of *Gclm*, *Gclc*, and *Slc7a11* (Fig. 3, *B* and *C*). Indeed, the protein amount of GCLM was higher in *Bach1*$^{-/-}$ MEFs than in WT cells (Fig. 3, *D* and *E*, and Fig. S4, *A* and *B*). However, the protein amounts of GCLC and SLC7A11 were similar between WT and *Bach1*$^{-/-}$ MEFs (Fig. 3, *D* and *E*, and Fig. S4, *A* and *B*). Cells may have additional mechanisms to tune strictly the protein amounts of GCLC and SLC7A11, managing the intracellular GSH amount and maintaining homeostasis. We found that SLC7A11 was further regulated by proteasomal degradation (Fig. 3, *D* and *E*). This observation suggests that the decision to undergo ferroptosis may be made based upon whether or not cells can induce efficiently inhibitory proteins like SLC7A11. Cells with higher amounts of SLC7A11 may likely be protected from ferroptosis. *Gclc* and *Slc7a11* may be critical factors for cells, with the transcriptional regulation by BACH1 and additional layers of regulation, although these points will need to be explored in further studies.

Reports on the function of HO-1 are conflicting, with studies conversely describing it to promote or inhibit ferroptosis (7, 26, 27, 63). These discrepant findings may be because HO-1 degrades prooxidant heme to produce not only the radical scavengers biliverdin and bilirubin but also free iron that mediates ferroptosis through Fenton reaction (14, 25). Therefore, to allow HO-1 to function effectively as an anti-oxidative stress enzyme, it is essential to suppress the reactivity of labile iron derived from heme. We showed that BACH1 represses the expression of the genes of ferritin and ferroportin (Fig. 4, *A* and *B*), both of which reduce the intracellular availability of labile iron. By increasing the expression of not only HO-1 but also ferritin and ferroportin during the induction of ferroptosis (Fig. 1*A*), the prooxidant activities of heme and heme-derived free iron can be suppressed efficiently, thus protecting cells from ferroptosis. Conversely, BACH1 represses the expression of ferritin and ferroportin in addition to HO-1, thus effectively promoting ferroptosis (Fig. 4*E*). Indeed, we showed *Bach1*$^{-/-}$ MEFs were more resistant to the elevation of mitochondrial labile iron than WT MEFs during ferroptosis (Fig. 4, *C* and *D*). Based on the present and previous findings, we proposed a model in which BACH1 accelerates ferroptosis by suppressing two major intracellular counteracting mechanisms against ferroptosis: the GSH synthesis pathway and the system for the sequestration of labile iron (Fig. 4*E*).

In addition, we showed that ferroptosis was involved in the pathology of not only ischemia-reperfusion injury (3, 4, 7) but also AMI. The severity of AMI was improved by the iron chela-

Figure 4. BACH1 increases mitochondrial labile iron during ferroptosis by repressing the transcription of genes of ferritin and ferroportin. *A,* qPCR analysis for *Fth1*, *Ftl1*, and *Slc40a1* mRNA relative to *Actb* mRNA in WT and *Bach1*$^{-/-}$ MEFs (7th, 9th, and 11th passage: P7, P9, and P11). $n = 3$ of independent lots of MEFs per genotype. *B,* ChIP-seq analysis of the binding of BACH1, MAFK for gene regions of *Fth1*, *Ftl1*, and *Slc40a1* in M1 cells. *C* and *D,* WT and *Bach1*$^{-/-}$ MEFs (P8) were exposed to erastin for 24 h and afterward, stained by Mito-FerroGreen, a fluorophore. Representative flow cytometry images (*C*) showing the strategy that was implemented for the sorting of Mito-FerroGreen positive cells. The positive cells were judged as mitochondrial-labile iron positive cells. Quantification of mitochondrial-labile iron (*D*). *MFI*, mean fluorescence intensity. *E,* conceptual diagram. *Error bars* of *A* and *D* represent S.D. *p* value of *A* by *t* test. *p* value of *D* by Tukey's test after two-way ANOVA.

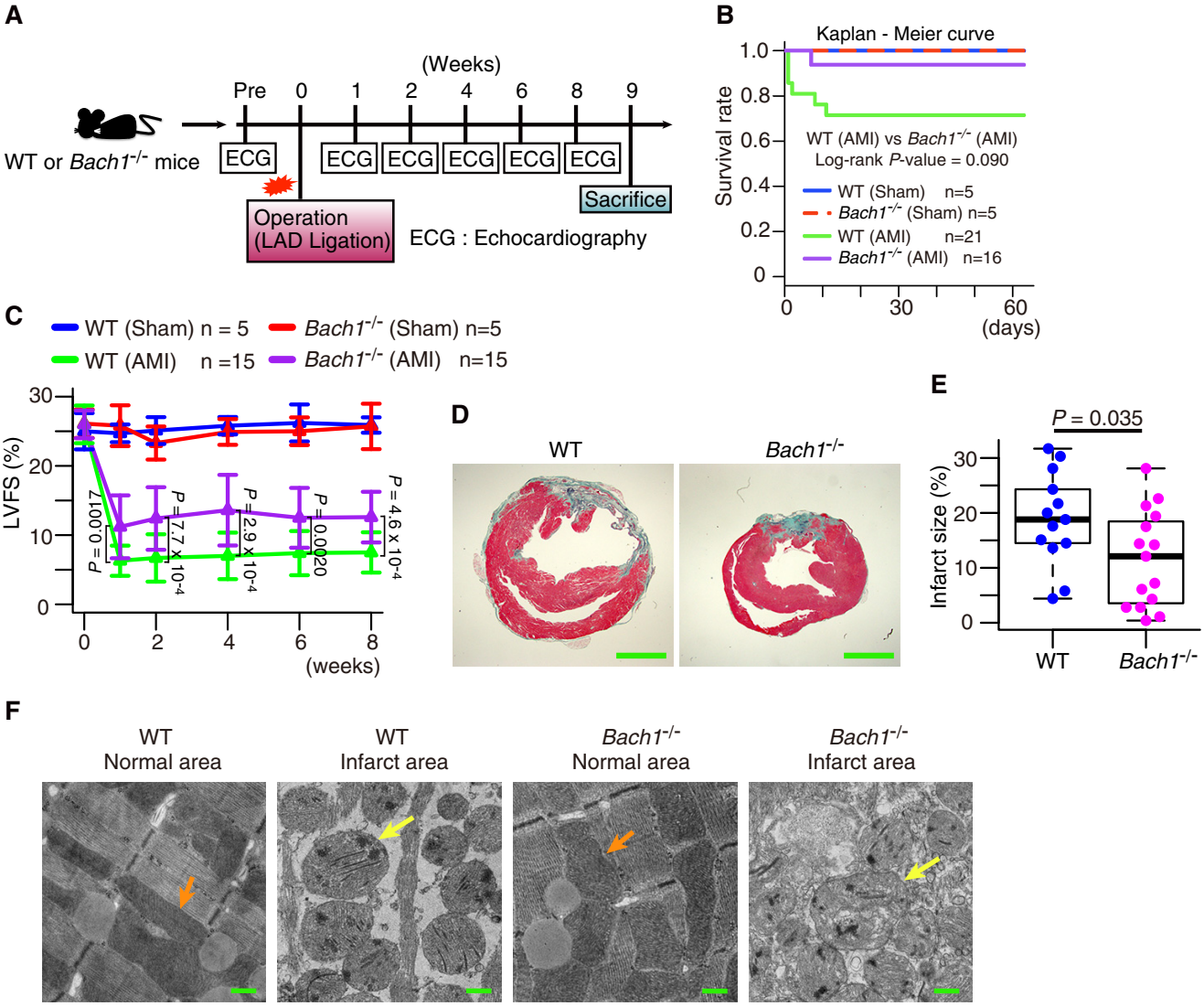

Figure 5. BACH1 aggravates AMI. *A,* experimental process. *B,* Kaplan-Meier curve of each group. *C,* left ventricular fractional shortening (*LVFS*) on echocardiogram. *D* and *E,* mice was dissected after 9 weeks from operation. *D*, representative photographs of heart sections stained with elastica Masson staining. *E*, infarct size to left ventricular section. *Scale bars* in *D* represent 2 mm. *F,* mice was dissected next day from operation. Transmission electron microscope image of normal and infarct area of hearts of mice next day from operation. *Orange arrow*: normal mitochondria. *Yellow arrow*: mitochondrial spheroid-like abnormality. *Scale bars* represent 500 nm. *Error bars* of *C* represent S.D. The *box and whisker plots* of *E* show the 25th and 75th percentile quartiles and median values (*center black line*) and maximum and minimum values of the data. *p* value of *B* by log-rank test between WT (AMI) and *Bach1*$^{-/-}$ (AMI). *p* value of *C* by Tukey-Kramer method after two-way ANOVA. *p* value of *E* by *t* test.

tor, DFX particularly in WT mice (Fig. 6, *C–F*). The peripheral areas of AMI are naturally reperfused by angiogenesis, where ferroptosis is likely induced. Our results here suggest that the therapeutic effect of DFX is expected in AMI and ischemia-reperfusion injury. Necroptosis is also reportedly involved in cardiac ischemic disease (64, 65). Therefore, the double inhibition of ferroptosis and necroptosis may lead to a more effective treatment of AMI. In addition, this study suggests that *Bach1*$^{-/-}$ mice are more resistant to AMI than WT mice because of their lower rate of ferroptosis than in WT mice (Figs. 5 and 6). BACH1 may be a potential therapeutic target of AMI in the future.

Ferroptosis is thought to play a major role in cancer suppression (2, 10). Our results suggest that cancer cells may acquire resistance against ferroptosis by decreasing BACH1 protein, thus eluding elimination by ferroptosis. We previously reported that BACH1 promotes the proliferation of MEFs transformed with H-Ras^{V12} and their tumor formation in a mouse transplantation model (66). Recently, BACH1 was found to promote the proliferation and/or metastasis of breast cancer, ovarian cancer, and lung cancer cells (48, 49, 67–70). BACH1 is therefore considered to have dual functions in cancers: promoting cell proliferation and cell death through ferroptosis. Cancer cells may adapt to their surrounding environment by changing the expression of BACH1; cancer cells may highly express BACH1 during stages of proliferation and metastasis but may reduce their levels of BACH1 under stress conditions, such as toxicity due to anti-cancer drugs. Such flexibility in the amount of BACH1 protein expressed may enhance the malignancy of cancer cells. Therapy that targets this flexibility, such as the down-regulation of BACH1 in response to erastin, may expand the field of potential cancer treatments.

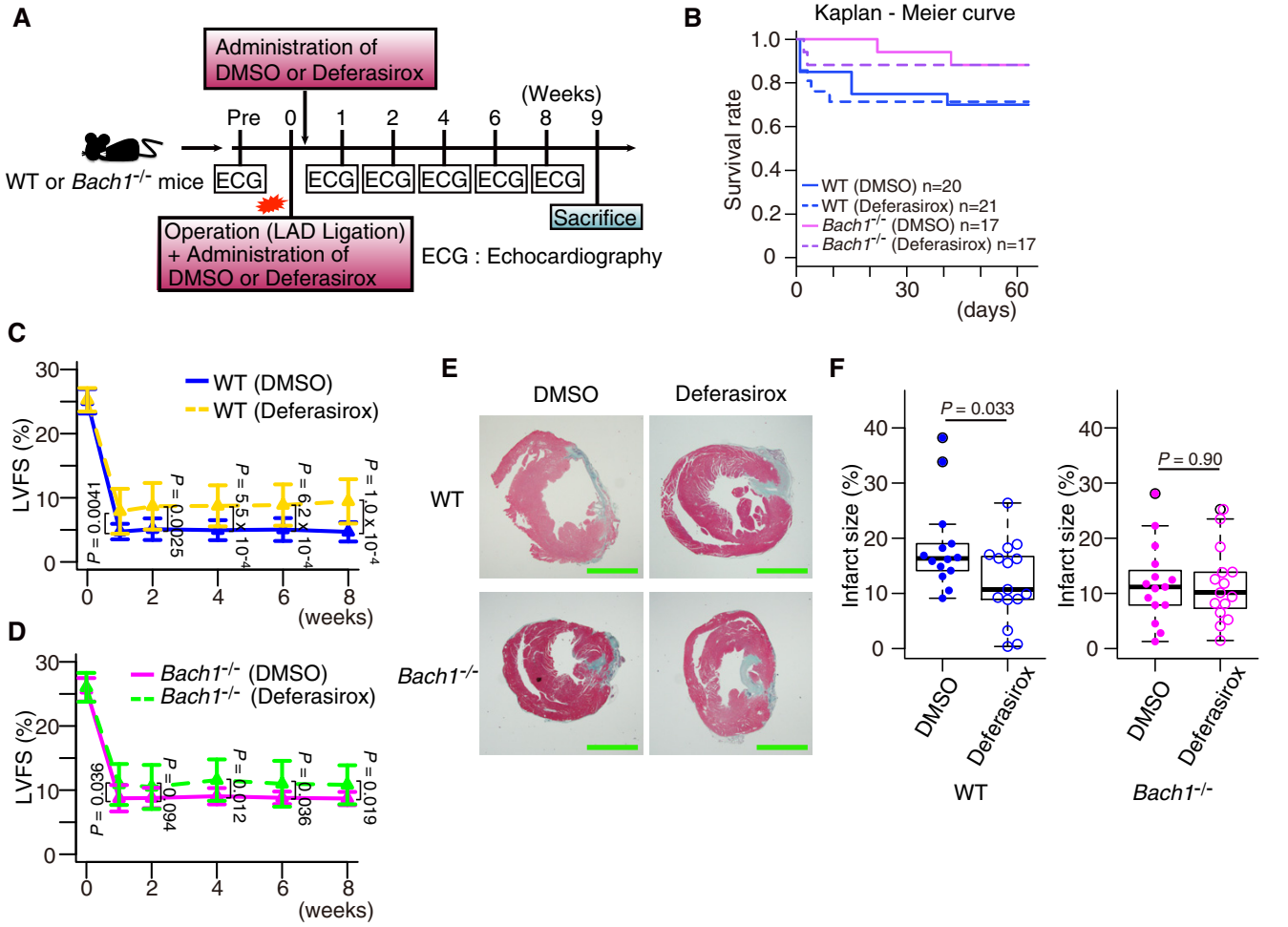

Figure 6. An iron chelator DFX alleviates AMI. *A,* experimental process. *B,* Kaplan-Meier curve of each group. *C* and *D,* left ventricular fractional shortening (*LVFS*) of WT mice (*C*) and *Bach1*$^{-/-}$ mice (*D*) on echocardiogram. *E* and *F,* mice were dissected after 9 weeks from operation. *E,* representative photographs of heart sections stained with elastica Masson staining. F, infarct size to left ventricular section. *Scale bars* in *E* represent 2 mm. *Error bars* of *C* and *D* represent S.D. The *box and whisker plots* of *F* show the 25th and 75th percentile quartiles and median values (*center black line*) and maximum and minimum values of the data. *p* value of *C, D,* and *F* by *t* test.

Experimental procedures

Mice

The generation of *Bach1*$^{-/-}$ mice on the C57BL/6J background was described previously (15). Mice 13 weeks of age were analyzed for models of AMI. Animals were euthanized by cervical dislocation under anesthetic inhalation overdose with isoflurane before anatomy. These mice were bred at the animal facility of Tohoku University. Mice were housed under specific pathogen-free conditions. All experiments performed in this study were approved by the Institutional Animal Care and Use Committee of the Tohoku University Environmental and Safety Committee.

Mice models of AMI

Induction of AMI was performed as described previously (43, 44). The mice were subjected to ligation of the proximal LAD to induce AMI. They were randomly assigned to sham or AMI (Fig. 5*A*), DMSO, or DFX groups (Fig. 6*A*). To follow up the time course of LV function after AMI, we performed transthoracic two-dimensional echocardiography. For histological analysis and analysis with transmission electron microscope, the heart was divided along the short axis at the center of the infarct.

Histopathological analysis

Excised hearts were fixed with 4% paraformaldehyde for histological and immunohistochemical examination. After 24–48 h of fixation and dehydration through increasing concentrations of ethanol, the tissue specimens were embedded in paraffin and sliced at 3 μm in thickness. The sections were used for Elastica-Masson staining. The extent of infarct area was calculated as a rate of fibrotic area using the following formula: fibrotic area/(LV free wall + interventricular septum) × 100 (%) with use of Photoshop software (Adobe).

Transmission electron microscopy

Cells and hearts were treated in 2.5% glutaraldehyde in 0.1 M cacodylate buffer (pH 7.4) for at least 24 h, and washed with 0.1 M cacodylate buffer 4 times and then treated with 1% OsO_4 in 0.1 M cacodylate buffer for 90 min. After dehydration through an ethanol series (50–100% ethanol), cells were embedded in Epon resin. Thin sections were cut with a microtome (Leica EM

UC-7), stained with 2% uranyl acetate and 0.4% lead citrate, and examined and photographed under a transmission electron microscope (Hitachi High-Technologies H-7600).

Isolation and culture of MEFs

MEFs were derived from 13.5-day-old embryos of WT or *Bach1*$^{-/-}$ mice. Following removal of the head and organs, embryos were rinsed with PBS (Nissui, Tokyo, Japan), minced and digested with trypsin (0.05% (v/v) solution containing 0.53 mM EDTA) (Gibco), and 1.8 mg/ml of DNase I (Roche, Basel, Switzerland) in PBS and incubated for 60 min at 37 °C. Trypsin was inactivated by addition of Dulbecco's modified Eagle's medium with high glucose (Gibco) containing 10% (v/v) fetal bovine serum (Sigma-Aldrich), 1× minimal essential medium nonessential amino acids (Gibco), and 0.1 mM 2-mercaptoethanol (Sigma-Aldrich). MEFs from a single embryo were plated into a 100-mm diameter culture dish and incubated at 37 °C in 3% oxygen (1st passage: P1). MEFs from embryos of homosexual littermates were mixed at 2nd passage (P2) and stocked.

MEFs were maintained at 37 °C in culture medium (Dulbecco's modified Eagle's medium with (Gibco) containing 10% fetal bovine serum (Sigma-Aldrich), 1× minimal essential medium nonessential amino acids (Gibco), penicillin/streptomycin (100 units/ml and 100 μg/ml each) (Gibco) and 0.1 mM 2-mercaptoethanol (Sigma-Aldrich)) in 3% oxygen for experiments. The number of passages were recorded for each lot of MEFs. From 5th to 11th passage MEFs were used for all experiments.

Reagents

Erastin, DMSO, and DFO were purchased from Sigma-Aldrich. MG132 was purchased from Calbiochem (San Diego, CA). DFX was transferred as raw material from Novartis Pfarma (Basel, Switzerland). *S*-Adenosylmethionine-$^{13}C_5$,^{15}N, and GSH-$^{13}C_2$,^{15}N were purchased from Taiyo Nissan Corp. (Tokyo, Japan) and used as internal standard for MS. Methanol, acetonitrile, and ammonium hydroxide for MS were purchased from Kanto Chemical (Tokyo, Japan). Ammonium bicarbonate (1 mol/liter) for MS was purchased from Cell Science and Technology Institute, Inc. (Miyagi, Japan). Formic acid for MS was purchased from Wako Pure Chemical Industries (Osaka, Japan).

Sample preparation for UHPLC/MS/MS

MEFs (3–8 × 10^6 cells for each lot) were suspended in 100 μl of methanol containing the internal standards (0.2 μg/ml of *S*-adenosylmethionine-$^{13}C_5$,^{15}N for positive ion mode (Pos) and 1 μg/ml of GSH-$^{13}C_2$,^{15}N for negative ion mode (Neg)), and were homogenized by mixing for 30 s followed by sonication for 10 min. After centrifugation at 16,400 × *g* for 20 min at 4 °C followed by deproteinization, 3 μl of each extract was analyzed by ultra HPLC triple quadrupole MS (UHPLC/MS/MS).

UHPLC/MS/MS analysis

The UHPLC/MS/MS analysis was performed on an Acquity™ Ultra Performance LC I-class system (Waters Corp., Milford, UK) interfaced to a Waters Xevo TQ-S MS/MS system equipped with electrospray ionization. The MS/MS was performed using the multiple reaction monitoring mode with a scan time of 1 ms for each compound. The transitions of the precursor ion to the product ion, cone voltage, and collision energy are listed in Table S1. The other settings are as follows: 3.5 kV (Pos) or 2.5 kV (Neg) capillary voltage, 30 V cone voltage, 50 V source offset, source temperature at 150 °C, 150 liter/h of cone gas (N_2) flow rate, desolvation temperature at 450 °C, 1000 liter/h of desolvation gas flow, 0.15 min/ml of collision gas flow, 7.00 bar nebulization gas (N_2) flow. LC separation was performed as described before (71), using a normal-phase column (ZIC-pHILIC; 100 × 2.1 mm inner diameter, 5-μm particle size; Sequant, Darmstadt, Germany) with a gradient elution using solvent A (10 mmol/liter of NH_4HCO_3, adjusted to pH 9.2 using ammonia solution) and B (acetonitrile) at 300 μl/min: 99 to 70% B from 0.5 to 4.0 min, 70 to 1% B from 4.0 to 6.5 min, 1% B for 2.5 min, and 99% B for 9 min until the end of the run. The oven temperature was 20 °C. The data were collected using the MassLynx version 4.1 software (Waters Corp.) and the ratio of the peak area of analyte to the internal standard was analyzed by Traverse MS (Reifycs Inc., Tokyo, Japan).

RNA interference

All siRNAs (siControl: Stealth RNAi™ siRNA Negative Control, Med GC; si*Gclm* #1: MSS204722; si*Gclm* #3: MSS204724; si*Slc7a11* #1: MSS218649; si*Slc7a11* #2: MSS218650; si*Gclc* #2: MSS204720; si*Gclc* #3: MSS204721; si*Hmox1* #1: MSS247281; si*Hmox1* #3: MSS274857) were obtained from Invitrogen. Sequences of the siRNAs are described in Table S2. 2 × 10^6 cells of MEFs were transfected with 1.2 nM siRNAs using Amaxa Nucleofector II (Lonza, Basel, Switzerland) and MF 1 Nucleofector kit (Lonza) according to the manufacturer's protocols. After transfection, MEFs were passaged to dishes or culture plate with culture medium.

Western blotting

Cells were trypsinized, pelleted, and washed twice in PBS. Cells were lysed beyond 5 min in SDS sample buffer (62.5 mM Tris-HCl (pH 6.8), 1% (v/v) 2-mercaptoethanol, 1% (w/v) SDS, 10% (w/v) glycerol, 0.02% (w/v) bromphenol blue). Lysates were resolved on 7.5–10% SDS-PAGE gels and transferred to polyvinylidene difluoride membranes (Millipore). The antibody for detection of β-actin (sc-1616) was purchased from Santa Cruz Biotechnology (Santa Cruz, CA). The antibody for detection of HO-1 (ADI-SPA-896) was purchased from Enzo Life Science (New York). The antibodies for GAPDH (ab8245), Gclc (ab53179), and Gclm (ab124827) were purchased from Abcam (Cambridge, UK). The antibody for Slc7a11 (119-11215) was purchased by RayBiotech (Norcross, GA). The antibody for BACH1 was described previously (15). For the quantification of signals, all samples to be compared were run on the same gel. Bands were quantified using ImageJ (72, 73). All bands to be compared were quantified on the same image and were within the linear range of detection of the software.

Quantitative PCR with reverse transcription

Total RNA was purified with RNeasy plus micro kit or RNeasy plus mini kit (Qiagen, Hilden, Germany). Complementary DNA was synthesized by a SuperScript III First-Strand Synthesis System (Invitrogen). Quantitative PCR was per-

formed using LightCycler Fast Start DNA Master SYBR Green I, and LightCycler nano (Roche) or LightCycler 96 (Roche). mRNA transcript abundance was normalized to that of Actb. Sequences of the qPCR primers are described in Table S3.

Administration of erastin and cell death assessment by flow cytometry

Before administration of erastin, the medium was exchanged to the experimental medium (culture medium without 2-mercaptoethanol and penicillin/streptomycin). Erastin was dissolved in DMSO and administered to experimental medium with DMSO. The concentration of DMSO was adjusted among each samples. Cell death was assessed 24 h after administration of erastin. PI and Annexin V staining were used for assessment of cell death. APC-Annexin V was purchased from BD Bioscience (Franklin Lakes, NJ). MEFs were stained by APC-Annexin V according to the manufacturer's protocols. PI was added to aliquot (1 μg/ml) before flow cytometry. The MEFs were sorted with a FACS Aria II (BD) and analyzed by FlowJo software (Tree Star, Ashland, OR). MEFs of positive, of whether at least Annexin V or PI, was assessed as dead cells. The gating strategy for assessing dead cells (Figs. 2, *B* and *E*; 4, *C* and *D*; and Figs. S3*B*, S7, *A*–*D*, S9*B*, and S10*E*) was shown in Fig. S2.

ChIP-Seq

We used ChIP-seq data of BACH1 and MAFK in the M1 cell line from GEO (Gene Expression Ominibus) data set GSE79139 that deposited for our previous report (34, 35).

Detection of mitochondrial labile iron

To detect mitochondrial labile iron, a fluorophore Mito-FerroGreen (Dojindo, Kumamoto, Japan) (39) was used according to the manufacturer's protocol. MEFs on 12-well plates (Corning, NY) were washed three times with Hank's balanced salt solution (HBSS) (Gibco) to remove the residual medium. Then MEFs were treated with 5 μM Mito-FerroGreen with HBSS for 30 min at 37 °C. After incubation, Mito-FerroGreen was removed by washing twice with HBSS. MEFs were stained by APC-Annexin V and PI, and sorted with a FACS Aria II (BD Bioscience) and analyzed by FlowJo software (Tree Star). MEFs that were negative for both Annexin V and PI were sorted as alive cells (Fig. 4, *C* and *D*). The gating strategy was shown in Fig. S2.

RNA-Seq

Total RNA was purified using an RNeasy plus mini kit (Qiagen). To remove ribosomal RNA (rRNA), 4 μg of the total RNA was treated with a GeneRead rRNA Depletion kit (Qiagen) and then with an RNeasy MiniElute kit (Qiagen) for cleanup. For fragmentation, 100 ng of the rRNA-depleted RNA was incubated at 95 °C for 10 min and purified by a Magnetic Beads Cleanup Module (Thermo Fisher Scientific, Carlsbad, CA). The libraries were constructed with an RNA-seq library kit version 2 (Thermo Fisher Scientific) on ABI library builder (Thermo Fisher Scientific), and was barcoded with Ion Xpress RNA-seq BC primer (Thermo Fisher Scientific). The library fragments with a size range of 100–200 bp were selected with Agencourt AMPure XP beads (Beckman Coulter, Brea, CA). Templates were prepared on the Ion Chef system using an Ion PI Hi-Q Chef kit (Thermo Fisher Scientific) and sequencing was performed on an Ion Proton system using the Ion PI Hi-Q sequencing kit (Thermo Fisher Scientific) and the PI v3 chip (Thermo Fisher Scientific). The sequence data were obtained as fastq files. The sequence data were aligned to reference hg19 using the RNASeq Analysis plugin from Ion torrent suite software (Thermo Fisher Scientific). Mapped reads were counted for each gene using HTSeq version 0.9.1 htseq-count. The differential expression analysis was performed on edge R version 3.16.5 after removal of low count lead genes using three biological replicates for each condition (less than 5 leads per gene in the sample and counts per million mapped reads (cpm) of 1 or less).

Statistics

For all experiments, differences of data sets were considered statistically significant when p values were lower than 0.05. Statistical comparisons were performed using the t test in comparison between the two groups, and one-, two-, or three-way ANOVA followed by Tukey's test or Tukey-Kramer method in comparison among multiple groups. For the t test, Student's t test was used when the S.D. of the groups was not significantly different by f test. Welch's t test was used when the S.D. of the groups was significantly different by f test.

Author contributions—H. N., M. M., and K. I. conceptualization; H. N., H. K., K. S., M. S., and Y. I. resources; H. N. formal analysis; H. N. validation; H. N., M. M., and D. S. investigation; H. N., M. M., T. S., D. S., H. S., and K. I. methodology; H. N. writing-original draft; M. M. and K. I. funding acquisition; K. I. supervision; K. I. project administration; K. I. writing-review and editing.

Acknowledgments—We thank members of the Department of Biochemistry, Tohoku University Graduate School of Medicine, for discussions and support and the Biomedical Research Core of Tohoku University Graduate School of Medicine for technical support. We thank Novartis for the raw material transfer of DFX for this study.

References

1. Dixon, S. J., Lemberg, K. M., Lamprecht, M. R., Skouta, R., Zaitsev, E. M., Gleason, C. E., Patel, D. N., Bauer, A. J., Cantley, A. M., Yang, W. S., Morrison, B., 3rd, Stockwell, B. R. (2012) Ferroptosis: an iron-dependent form of nonapoptotic cell death. *Cell* **149,** 1060–1072 CrossRef Medline
2. Yang, W. S., SriRamaratnam, R., Welsch, M. E., Shimada, K., Skouta, R., Viswanathan, V. S., Cheah, J. H., Clemons, P. A., Shamji, A. F., Clish, C. B., Brown, L. M., Girotti, A. W., Cornish, V. W., Schreiber, S. L., and Stockwell, B. R. (2014) Regulation of ferroptotic cancer cell death by GPX4. *Cell* **156,** 317–331 CrossRef Medline
3. Gao, M., Monian, P., Quadri, N., Ramasamy, R., and Jiang, X. (2015) Glutaminolysis and transferrin regulate ferroptosis. *Mol. Cell* **59,** 298–308 CrossRef Medline
4. Baba, Y., Higa, J. K., Shimada, B. K., Horiuchi, K. M., Suhara, T., Kobayashi, M., Woo, J. D., Aoyagi, H., Marh, K. S., Kitaoka, H., and Matsui, T. (2018) Protective effects of the mechanistic target of rapamycin against excess iron and ferroptosis in cardiomyocytes. *Am. J. Physiol. Heart Circ. Physiol.* **314,** H659–H668 CrossRef Medline
5. Linkermann, A., Bäasen, J. H., Darding, M., Jin, M. K., Sanz, A. B., Heller, J. O., De Zen, F., Weinlich, R., Ortiz, A., Walczak, H., Weinberg, J. M., Green, D. R., Kunzendorf, U., and Krautwald, S. (2013) Two independent pathways of regulated necrosis mediate ischemia-reperfusion injury. *Proc. Natl. Acad. Sci. U.S.A.* **110,** 12024–12029 CrossRef Medline

6. Linkermann, A., Skouta, R., Himmerkus, N., Mulay, S. R., Dewitz, C., De Zen, F., Prokai, A., Zuchtriegel, G., Krombach, F., Welz, P. S., Weinlich, R., Vanden Berghe, T., Vandenabeele, P., Pasparakis, M., Bleich, M., *et al.* (2014) Synchronized renal tubular cell death involves ferroptosis. *Proc. Natl. Acad. Sci. U.S.A.* **111,** 16836–16841 CrossRef Medline
7. Fang, X., Wang, H., Han, D., Xie, E., Yang, X., Wei, J., Gu, S., Gao, F., Zhu, N., Yin, X., Cheng, Q., Zhang, P., Dai, W., Chen, J., Yang, F., Yang, H. T., Linkermann, A., Gu, W., Min, J., and Wang, F. (2019) Ferroptosis as a target for protection against cardiomyopathy. *Proc. Natl. Acad. Sci. U.S.A.* **116,** 2672–2680 CrossRef Medline
8. Chiang, G. C., Mao, X., Kang, G., Chang, E., Pandya, S., Vallabhajosula, S., Isaacson, R., Ravdin, L. D., Alzheimer's Disease Neuroimaging Initiative, and Shungu, D. C. (2017) Relationships among cortical glutathione levels, brain amyloidosis, and memory in healthy older adults investigated *in vivo* with ^{1}H-MRS and Pittsburgh compound-B PET. *Am. J. Neuroradiol.* **38,** 1130–1137 CrossRef Medline
9. Di Domenico, F., Tramutola, A., and Butterfield, D. A. (2017) Role of 4-hydroxy-2-nonenal (HNE) in the pathogenesis of Alzheimer disease and other selected age-related neurodegenerative disorders. *Free Radic. Biol. Med.* **111,** 253–261 CrossRef Medline
10. Jiang, L., Kon, N., Li, T., Wang, S. J., Su, T., Hibshoosh, H., Baer, R., and Gu, W. (2015) Ferroptosis as a p53-mediated activity during tumour suppression. *Nature* **520,** 57–62 CrossRef Medline
11. Kim, S. E., Zhang, L., Ma, K., Riegman, M., Chen, F., Ingold, I., Conrad, M., Turker, M. Z., Gao, M., Jiang, X., Monette, S., Pauliah, M., Gonen, M., Zanzonico, P., Quinn, T., Wiesner, U., Bradbury, M. S., and Overholtzer, M. (2016) Ultrasmall nanoparticles induce ferroptosis in nutrient-deprived cancer cells and suppress tumour growth. *Nat. Nanotechnol.* **11,** 977–985 CrossRef Medline
12. Viswanathan, V. S., Ryan, M. J., Dhruv, H. D., Gill, S., Eichhoff, O. M., Seashore-Ludlow, B., Kaffenberger, S. D., Eaton, J. K., Shimada, K., Aguirre, A. J., Viswanathan, S. R., Chattopadhyay, S., Tamayo, P., Yang, W. S., Rees, M. G., *et al.* (2017) Dependency of a therapy-resistant state of cancer cells on a lipid peroxidase pathway. *Nature* **547,** 453–457 CrossRef Medline
13. Hangauer, M. J., Viswanathan, V. S., Ryan, M. J., Bole, D., Eaton, J. K., Matov, A., Galeas, J., Dhruv, H. D., Berens, M. E., Schreiber, S. L., McCormick, F., and McManus, M. T. (2017) Drug-tolerant persister cancer cells are vulnerable to GPX4 inhibition. *Nature* **551,** 247–250 CrossRef Medline
14. Igarashi, K., and Watanabe-Matsui, M. (2014) Wearing red for signaling: the heme-bach axis in heme metabolism, oxidative stress response and iron immunology. *Tohoku J. Exp. Med.* **232,** 229–253 CrossRef Medline
15. Sun, J., Hoshino, H., Takaku, K., Nakajima, O., Muto, A., Suzuki, H., Tashiro, S., Takahashi, S., Shibahara, S., Alam, J., Taketo, M. M., Yamamoto, M., and Igarashi, K. (2002) Hemoprotein Bach1 regulates enhancer availability of heme oxygenase-1 gene. *EMBO J.* **21,** 5216–5224 CrossRef Medline
16. Hintze, K. J., Katoh, Y., Igarashi, K., and Theil, E. C. (2007) Bach1 repression of ferritin and thioredoxin reductase1 is heme-sensitive in cells and *in vitro* and coordinates expression with heme oxygenase1, β-globin, and NADP(H) quinone (oxido) reductase 1. *J. Biol. Chem.* **282,** 34365–34371 CrossRef Medline
17. Warnatz, H. J., Schmidt, D., Manke, T., Piccini, I., Sultan, M., Borodina, T., Balzereit, D., Wruck, W., Soldatov, A., Vingron, M., Lehrach, H., and Yaspo, M. L. (2011) The BTB and CNC homology 1 (BACH1) target genes are involved in the oxidative stress response and in control of the cell cycle. *J. Biol. Chem.* **286,** 23521–23532 CrossRef Medline
18. Yano, Y., Ozono, R., Oishi, Y., Kambe, M., Yoshizumi, M., Ishida, T., Omura, S., Oshima, T., and Igarashi, K. (2006) Genetic ablation of the transcription repressor Bach1 leads to myocardial protection against ischemia/reperfusion in mice. *Genes Cells* **11,** 791–803 CrossRef
19. Ito, M., Nagano, N., Arai, Y., Ogawa, R., Kobayashi, S., Motojima, Y., Go, H., Tamura, M., Igarashi, K., Dennery, P. A., and Namba, F. (2017) Genetic ablation of Bach1 gene enhances recovery from hyperoxic lung injury in newborn mice via transient upregulation of inflammatory genes. *Pediatr. Res.* **81,** 926–931 CrossRef Medline
20. Harusato, A., Naito, Y., Takagi, T., Uchiyama, K., Mizushima, K., Hirai, Y., Higashimura, Y., Katada, K., Handa, O., Ishikawa, T., Yagi, N., Kokura, S., Ichikawa, H., Muto, A., Igarashi, K., and Yoshikawa, T. (2013) BTB and CNC homolog 1 (Bach1) deficiency ameliorates TNBS colitis in mice: role of M2 macrophages and heme oxygenase-1. *Inflamm. Bowel Dis.* **19,** 740–753 CrossRef Medline
21. Inoue, M., Tazuma, S., Kanno, K., Hyogo, H., Igarashi, K., and Chayama, K. (2011) Bach1 gene ablation reduces steatohepatitis in mouse MCD diet model. *J. Clin. Biochem. Nutri.* **48,** 161–166 Medline
22. Kanno, H., Ozawa, H., Dohi, Y., Sekiguchi, A., Igarashi, K., and Itoi, E. (2009) Genetic ablation of transcription repressor Bach1 reduces neural tissue damage and improves locomotor function after spinal cord injury in mice. *J. Neurotrauma* **26,** 31–39 CrossRef Medline
23. Shimada, K., Skouta, R., Kaplan, A., Yang, W. S., Hayano, M., Dixon, S. J., Brown, L. M., Valenzuela, C. A., Wolpaw, A. J., and Stockwell, B. R. (2016) Global survey of cell death mechanisms reveals metabolic regulation of ferroptosis. *Nat. Chem. Biol.* **12,** 497–503 CrossRef Medline
24. Yang, W. S., Kim, K. J., Gaschler, M. M., Patel, M., Shchepinov, M. S., and Stockwell, B. R. (2016) Peroxidation of polyunsaturated fatty acids by lipoxygenases drives ferroptosis. *Proc. Natl. Acad. Sci. U.S.A.* **113,** E4966–E4975 CrossRef Medline
25. Stockwell, B. R., Friedmann Angeli, J. P., Bayir, H., Bush, A. I., Conrad, M., Dixon, S. J., Fulda, S., Gascon, S., Hatzios, S. K., Kagan, V. E., Noel, K., Jiang, X., Linkermann, A., Murphy, M. E., Overholtzer, M., *et al.* (2017) Ferroptosis: a regulated cell death nexus linking metabolism, redox biology, and disease. *Cell* **171,** 273–285 CrossRef Medline
26. Kwon, M. Y., Park, E., Lee, S. J., and Chung, S. W. (2015) Heme oxygenase-1 accelerates erastin-induced ferroptotic cell death. *Oncotarget* **6,** 24393–24403 Medline
27. Sun, X., Ou, Z., Chen, R., Niu, X., Chen, D., Kang, R., and Tang, D. (2016) Activation of the p62-Keap1-NRF2 pathway protects against ferroptosis in hepatocellular carcinoma cells. *Hepatology (Baltimore, MD)* **63,** 173–184 CrossRef Medline
28. Sato, H., Tamba, M., Kuriyama-Matsumura, K., Okuno, S., and Bannai, S. (2000) Molecular cloning and expression of human xCT, the light chain of amino acid transport system xc. *Antioxid. Redox Signal.* **2,** 665–671 Medline
29. Sato, H., Shiiya, A., Kimata, M., Maebara, K., Tamba, M., Sakakura, Y., Makino, N., Sugiyama, F., Yagami, K., Moriguchi, T., Takahashi, S., and Bannai, S. (2005) Redox imbalance in cystine/glutamate transporter-deficient mice. *J. Biol. Chem.* **280,** 37423–37429 CrossRef Medline
30. Telorack, M., Abplanalp, J., and Werner, S. (2016) Low levels of glutathione are sufficient for survival of keratinocytes after UV irradiation and for healing of mouse skin wounds. *Arch. Dermatol. Res.* **308,** 443–448 CrossRef Medline
31. Fan, X., Liu, X., Hao, S., Wang, B., Robinson, M. L., and Monnier, V. M. (2012) The LEGSKO mouse: a mouse model of age-related nuclear cataract based on genetic suppression of lens glutathione synthesis. *PloS One* **7,** e50832 CrossRef Medline
32. Miess, H., Dankworth, B., Gouw, A. M., Rosenfeldt, M., Schmitz, W., Jiang, M., Saunders, B., Howell, M., Downward, J., Felsher, D. W., Peck, B., and Schulze, A. (2018) The glutathione redox system is essential to prevent ferroptosis caused by impaired lipid metabolism in clear cell renal cell carcinoma. *Oncogene* **37,** 5435–5450 CrossRef Medline
33. Ding, W. X., Li, M., Biazik, J. M., Morgan, D. G., Guo, F., Ni, H. M., Goheen, M., Eskelinen, E. L., and Yin, X. M. (2012) Electron microscopic analysis of a spherical mitochondrial structure. *J. Biol. Chem.* **287,** 42373–42378 CrossRef Medline
34. Ebina-Shibuya, R., Watanabe-Matsui, M., Matsumoto, M., Itoh-Nakadai, A., Funayama, R., Nakayama, K., Muto, A., and Igarashi, K. (2016) The double knockout of Bach1 and Bach2 in mice reveals shared compensatory mechanisms in regulating alveolar macrophage function and lung surfactant homeostasis. *J. Biochem.* **160,** 333–344 CrossRef Medline
35. Ebina-Shibuya, R., Matsumoto, M., Kuwahara, M., Jang, K. J., Sugai, M., Ito, Y., Funayama, R., Nakayama, K., Sato, Y., Ishii, N., Okamura, Y., Kinoshita, K., Kometani, K., Kurosaki, T., Muto, A., *et al.* (2017) Inflammatory responses induce an identity crisis of alveolar macrophages, leading

to pulmonary alveolar proteinosis. *J. Biol. Chem.* **292,** 18098–18112 CrossRef Medline
36. Wang, Y. Q., Chang, S. Y., Wu, Q., Gou, Y. J., Jia, L., Cui, Y. M., Yu, P., Shi, Z. H., Wu, W. S., Gao, G., and Chang, Y. Z. (2016) The protective role of mitochondrial ferritin on erastin-induced ferroptosis. *Front. Aging Neurosci.* **8,** 308 Medline
37. Hou, W., Xie, Y., Song, X., Sun, X., Lotze, M. T., Zeh H. J., 3rd, Kang, R., and Tang, D. (2016) Autophagy promotes ferroptosis by degradation of ferritin. *Autophagy* **12,** 1425–1428 CrossRef Medline
38. Geng, N., Shi, B. J., Li, S. L., Zhong, Z. Y., Li, Y. C., Xua, W. L., Zhou, H., and Cai, J. H. (2018) Knockdown of ferroportin accelerates erastin-induced ferroptosis in neuroblastoma cells. *Eur. Rev. Med. Pharmacol. Sci.* **22,** 3826–3836 Medline
39. Hirayama, T., Kadota, S., Niwa, M., and Nagasawa, H. (2018) A mitochondria-targeted fluorescent probe for selective detection of mitochondrial labile Fe(II). *Metallomics* **10,** 794–801 CrossRef
40. Starke, P. E., and Farber, J. L. (1985) Endogenous defenses against the cytotoxicity of hydrogen peroxide in cultured rat hepatocytes. *J. Biol. Chem.* **260,** 86–92 Medline
41. Kehrer, J. P. (2000) The Haber-Weiss reaction and mechanisms of toxicity. *Toxicology* **149,** 43–50 CrossRef Medline
42. Rauen, U., Petrat, F., Sustmann, R., and de Groot, H. (2004) Iron-induced mitochondrial permeability transition in cultured hepatocytes. *J. Hepatol.* **40,** 607–615 CrossRef Medline
43. Abarbanell, A. M., Herrmann, J. L., Weil, B. R., Wang, Y., Tan, J., Moberly, S. P., Fiege, J. W., and Meldrum, D. R. (2010) Animal models of myocardial and vascular injury. *J. Surg. Res.* **162,** 239–249 CrossRef Medline
44. Shindo, T., Ito, K., Ogata, T., Hatanaka, K., Kurosawa, R., Eguchi, K., Kagaya, Y., Hanawa, K., Aizawa, K., Shiroto, T., Kasukabe, S., Miyata, S., Taki, H., Hasegawa, H., Kanai, H., and Shimokawa, H. (2016) Low-intensity pulsed ultrasound enhances angiogenesis and ameliorates left ventricular dysfunction in a mouse model of acute myocardial infarction. *Arterioscler. Thromb. Vasc. Biol.* **36,** 1220–1229 CrossRef
45. Ogawa, K., Sun, J., Taketani, S., Nakajima, O., Nishitani, C., Sassa, S., Hayashi, N., Yamamoto, M., Shibahara, S., Fujita, H., and Igarashi, K. (2001) Heme mediates derepression of Maf recognition element through direct binding to transcription repressor Bach1. *EMBO J.* **20,** 2835–2843 CrossRef Medline
46. Zenke-Kawasaki, Y., Dohi, Y., Katoh, Y., Ikura, T., Ikura, M., Asahara, T., Tokunaga, F., Iwai, K., and Igarashi, K. (2007) Heme induces ubiquitination and degradation of the transcription factor Bach1. *Mol. Cell. Biol.* **27,** 6962–6971 CrossRef Medline
47. Ishikawa, M., Numazawa, S., and Yoshida, T. (2005) Redox regulation of the transcriptional repressor Bach1. *Free Radic. Biol. Med.* **38,** 1344–1352 CrossRef Medline
48. Wiel, C., Le Gal, K., Ibrahim, M. X., Jahangir, C. A., Kashif, M., Yao, H., Ziegler, D. V., Xu, X., Ghosh, T., Mondal, T., Kanduri, C., Lindahl, P., Sayin, V. I., and Bergo, M. O. (2019) BACH1 stabilization by antioxidants stimulates lung cancer metastasis. *Cell* **178,** 330–345.e22 CrossRef Medline
49. Lignitto, L., LeBoeuf, S. E., Homer, H., Jiang, S., Askenazi, M., Karakousi, T. R., Pass, H. I., Bhutkar, A. J., Tsirigos, A., Ueberheide, B., Sayin, V. I., Papagiannakopoulos, T., and Pagano, M. (2019) Nrf2 activation promotes lung cancer metastasis by inhibiting the degradation of Bach1. *Cell* **178,** 316–329.e18 CrossRef Medline
50. Marro, S., Chiabrando, D., Messana, E., Stolte, J., Turco, E., Tolosano, E., and Muckenthaler, M. U. (2010) Heme controls ferroportin1 (FPN1) transcription involving Bach1, Nrf2 and a MARE/ARE sequence motif at position −7007 of the FPN1 promoter. *Haematologica* **95,** 1261–1268 CrossRef Medline
51. Ishii, T., Itoh, K., Takahashi, S., Sato, H., Yanagawa, T., Katoh, Y., Bannai, S., and Yamamoto, M. (2000) Transcription factor Nrf2 coordinately regulates a group of oxidative stress-inducible genes in macrophages. *J. Biol. Chem.* **275,** 16023–16029 CrossRef Medline
52. Bea, F., Hudson, F. N., Chait, A., Kavanagh, T. J., and Rosenfeld, M. E. (2003) Induction of glutathione synthesis in macrophages by oxidized low-density lipoproteins is mediated by consensus antioxidant response elements. *Circ. Res.* **92,** 386–393 CrossRef Medline
53. Sekhar, K. R., Crooks, P. A., Sonar, V. N., Friedman, D. B., Chan, J. Y., Meredith, M. J., Starnes, J. H., Kelton, K. R., Summar, S. R., Sasi, S., and Freeman, M. L. (2003) NADPH oxidase activity is essential for Keap1/Nrf2-mediated induction of GCLC in response to 2-indol-3-yl-methylenequinuclidin-3-ols. *Cancer Res.* **63,** 5636–5645 Medline
54. Wild, A. C., Moinova, H. R., and Mulcahy, R. T. (1999) Regulation of γ-glutamylcysteine synthetase subunit gene expression by the transcription factor Nrf2. *J. Biol. Chem.* **274,** 33627–33636 CrossRef Medline
55. Sasaki, H., Sato, H., Kuriyama-Matsumura, K., Sato, K., Maebara, K., Wang, H., Tamba, M., Itoh, K., Yamamoto, M., and Bannai, S. (2002) Electrophile response element-mediated induction of the cystine/glutamate exchange transporter gene expression. *J. Biol. Chem.* **277,** 44765–44771 CrossRef Medline
56. Alam, J., Stewart, D., Touchard, C., Boinapally, S., Choi, A. M., and Cook, J. L. (1999) Nrf2, a Cap'n'Collar transcription factor, regulates induction of the heme oxygenase-1 gene. *J. Biol. Chem.* **274,** 26071–26078 CrossRef Medline
57. Cao, J. Y., Poddar, A., Magtanong, L., Lumb, J. H., Mileur, T. R., Reid, M. A., Dovey, C. M., Wang, J., Locasale, J. W., Stone, E., Cole, S. P. C., Carette, J. E., and Dixon, S. J. (2019) A genome-wide haploid genetic screen identifies regulators of glutathione abundance and ferroptosis sensitivity. *Cell Rep.* **26,** 1544–1556.e8 CrossRef Medline
58. Fan, Z., Wirth, A. K., Chen, D., Wruck, C. J., Rauh, M., Buchfelder, M., and Savaskan, N. (2017) Nrf2-Keap1 pathway promotes cell proliferation and diminishes ferroptosis. *Oncogenesis* **6,** e371 CrossRef Medline
59. Roh, J. L., Kim, E. H., Jang, H., and Shin, D. (2017) Nrf2 inhibition reverses the resistance of cisplatin-resistant head and neck cancer cells to artesunate-induced ferroptosis. *Redox Biol.* **11,** 254–262 CrossRef Medline
60. Lee, P. J., Jiang, B. H., Chin, B. Y., Iyer, N. V., Alam, J., Semenza, G. L., and Choi, A. M. (1997) Hypoxia-inducible factor-1 mediates transcriptional activation of the heme oxygenase-1 gene in response to hypoxia. *J. Biol. Chem.* **272,** 5375–5381 CrossRef Medline
61. Gong, P., Hu, B., Stewart, D., Ellerbe, M., Figueroa, Y. G., Blank, V., Beckman, B. S., and Alam, J. (2001) Cobalt induces heme oxygenase-1 expression by a hypoxia-inducible factor-independent mechanism in Chinese hamster ovary cells: regulation by Nrf2 and MafG transcription factors. *J. Biol. Chem.* **276,** 27018–27025 CrossRef Medline
62. Jiang, Y., Mao, C., Yang, R., Yan, B., Shi, Y., Liu, X., Lai, W., Liu, Y., Wang, X., Xiao, D., Zhou, H., Cheng, Y., Yu, F., Cao, Y., Liu, S., Yan, Q., and Tao, Y. (2017) EGLN1/c-Myc induced lymphoid-specific helicase inhibits ferroptosis through lipid metabolic gene expression changes. *Theranostics* **7,** 3293–3305 CrossRef Medline
63. Adedoyin, O., Boddu, R., Traylor, A., Lever, J. M., Bolisetty, S., George, J. F., and Agarwal, A. (2018) Heme oxygenase-1 mitigates ferroptosis in renal proximal tubule cells. *Am. J. Physiol. Renal Physiol.* **314,** F702–F714 CrossRef Medline
64. Smith, C. C., Davidson, S. M., Lim, S. Y., Simpkin, J. C., Hothersall, J. S., and Yellon, D. M. (2007) Necrostatin: a potentially novel cardioprotective agent? *Cardiovasc. Drugs Ther.* **21,** 227–233 CrossRef Medline
65. Oerlemans, M. I., Liu, J., Arslan, F., den Ouden, K., van Middelaar, B. J., Doevendans, P. A., and Sluijter, J. P. (2012) Inhibition of RIP1-dependent necrosis prevents adverse cardiac remodeling after myocardial ischemia-reperfusion *in vivo*. *Basic Res. Cardiol.* **107,** 270 CrossRef Medline
66. Nakanome, A., Brydun, A., Matsumoto, M., Ota, K., Funayama, R., Nakayama, K., Ono, M., Shiga, K., Kobayashi, T., and Igarashi, K. (2013) Bach1 is critical for the transformation of mouse embryonic fibroblasts by Ras(V12) and maintains ERK signaling. *Oncogene* **32,** 3231–3245 CrossRef Medline
67. Lee, J., Yesilkanal, A. E., Wynne, J. P., Frankenberger, C., Liu, J., Yan, J., Elbaz, M., Rabe, D. C., Rustandy, F. D., Tiwari, P., Grossman, E. A., Hart, P. C., Kang, C., Sanderson, S. M., Andrade, J., *et al.* (2019) Effective breast cancer combination therapy targeting BACH1 and mitochondrial metabolism. *Nature* **568,** 254–258 CrossRef Medline
68. Mansoori, B., Mohammadi, A., Asadzadeh, Z., Shirjang, S., Minouei, M., Abedi Gaballu, F., Shajari, N., Kazemi, T., Gjerstorff, M. F., Duijf, P. H. G., and Baradaran, B. (2019) HMGA2 and Bach-1 cooperate to promote breast cancer cell malignancy. *J. Cell. Physiol.* **234,** 17714–17726 Medline

69. Han, W., Zhang, Y., Niu, C., Guo, J., Li, J., Wei, X., Jia, M., Zhi, X., Yao, L., and Meng, D. (2019) BTB and CNC homology 1 (Bach1) promotes human ovarian cancer cell metastasis by HMGA2-mediated epithelial-mesenchymal transition. *Cancer Lett.* **445,** 45–56 CrossRef Medline
70. Lee, J., Lee, J., Farquhar, K. S., Yun, J., Frankenberger, C. A., Bevilacqua, E., Yeung, K., Kim, E. J., Balázsi, G., and Rosner, M. R. (2014) Network of mutually repressive metastasis regulators can promote cell heterogeneity and metastatic transitions. *Proc. Natl. Acad. Sci. U.S.A.* **111,** E364–E373 CrossRef Medline
71. Saigusa, D., Okamura, Y., Motoike, I. N., Katoh, Y., Kurosawa, Y., Saijyo, R., Koshiba, S., Yasuda, J., Motohashi, H., Sugawara, J., Tanabe, O., Kinoshita, K., and Yamamoto, M. (2016) Establishment of protocols for global metabolomics by LC-MS for biomarker discovery. *PloS One* **11,** e0160555 CrossRef Medline
72. Rasband, W. S. (1997–2012) *ImageJ*, U.S. National Institutes of Health, Bethesda, MD
73. Schneider, C. A., Rasband, W. S., and Eliceiri, K. W. (2012) NIH Image to ImageJ: 25 years of image analysis. *Nat. Methods* **9,** 671–675 CrossRef Medline